Studies on Combustion Behaviours of Single Biomass Particles Using a Visualization Method

Liang Shan[a, b], Ming Kong[b, c], Tom D. Bennet[b], Archi C. Sarroza[b], Carol Eastwick[b], Duo Sun[d], Gang Lu[d], Yong Yan[d], Hao Liu[b, 1]

a. College of Information Engineering, China Jiliang University, Hangzhou 310018, China
b. Faculty of Engineering, University of Nottingham, University Park, Nottingham, NG7 2RD, UK
c. College of Metrology and Measurement Engineering, China Jiliang University, Hangzhou 310018, China
d. School of Engineering and Digital Arts, University of Kent, Canterbury, Kent CT2 7NT, UK

Abstract

Combustion behaviours of single particles (125-150μm) of eucalyptus, pine and olive residue were investigated by means of a transparent visual drop-tube furnace, electrically heated to 1073 K, and a high-speed camera coupling with a long distance microscope. All three types of biomass samples were found to have two evident combustion phases, i.e., volatile combustion in an envelope flame and subsequent char combustion with high luminance. Yet, due to differences in chemical compositions and properties, their combustion behaviours were also seen somewhat discrepant. The volatile flame of the olive residue was fainter than that of pine and eucalyptus due to its high ash mass fraction. During the char combustion phase, fragmentation took place for most pine particles but only for a few particles of olive residue and eucalyptus. For all three types of biomass samples, the flame size and the average luminous intensity profiles were deduced from the captured combustion video images whilst the combustion burnout times of the volatile matter and char were also calculated and estimated. There were two peak values clearly shown on the profiles

[1] Corresponding author, Email: liu.hao@nottingham.ac.uk, Tel: +44 115 8467674

of both the flame size and the average luminous intensity during the volatile combustion process of pine and eucalyptus particles, which, according to literature, could not be observed by optical pyrometry. The observed peaks correspond to the devolatilisation of hemicellulose and cellulose. The ratio between the estimated char burnout time and volatile combustion time increases quadratically with the fixed carbon to volatile matter mass ratio, confirming char combustion is much slower than volatile combustion.

Key words: single biomass particle; combustion; visual drop-tube furnace; luminous intensity; flame imaging

1. Introduction

In recent decades, nations around the world have attached more importance to renewable energy resources such as biomass, taking them as a crucial part of the energy mix. In addition to various woody feedstock, biomass fuels also include all kinds of agricultural and forestry wastes, such as straw, sawdust, rice husks, peanut shells, bagasse, and animal waste as well as organic municipal solid waste. They are mainly composed of carbon, hydrogen, oxygen, nitrogen and other elements. Usually with high volatile matter mass fraction, high carbon reactivity, and low nitrogen, sulphur and ash mass fractions, biomass has a very short production/replantation cycle of a few years and hence is an ideal carbon-neutral replacement fuel for coal. However, biomass differs from coal in many aspects in terms of fuel properties and hence combustion behaviours. In addition, some properties such as moisture, volatile matter, ash and alkali metal mass fractions can significantly affect biomass combustion processes in terms of flame stability and combustion efficiency, and cause various operational problems such as fouling, slagging and corrosion of heat exchange tubes within the pulverised-fuel combustion boilers [1]. To understand the underlying causes of these problems, a profound understanding of the combustion characteristics and combustion kinetics of various biomass fuels is crucial.

Due to the prominent status in power generation, pulverized coal combustion has been the research focus for past several decades. Numerous scientific publications have been assembled detailing the ignition and combustion behaviours of individual coal particles [2-11]. The commonly used techniques include thermogravimetric analysis (TGA) [9], optical pyrometry [2-10], high-speed cinematography [2-6, 9], modelling [7, 11] and sometimes in conjunction with morphological examinations [2, 5, 9]. Over recent years, a number of studies on biomass particle ignition and combustion characteristics have sprung up, using the similar experimental setup and techniques to the coal particles [10, 12-25].

Toptas et al. [13] investigated the combustion behaviour of different kinds of torrefied biomass (lignocellulosic and animal wastes) and their blends with lignite via a non-isothermal TGA method in air. It was found that the ignition and burnout temperatures were reduced by blending biomass into the coal. Liu et al. [14] evaluated the combustion performance of one herbaceous biomass (corncob), one woody biomass (hardwood) and one bituminous coal using TGA and differential thermal gravity (DTG) analysis. The investigation focused on the influence of heating rates, blending ratios and sample kinds on the combustion behaviours and kinetics. Wei et al. [15] also investigated the combustion behaviours of anthracite coal/spent coffee grounds under oxy-fuel conditions by TGA and DTG analysis.

Levendis et al. [10] developed a three-colour ratio pyrometer to measure the surface temperatures and high-temperature combustion rates of burning carbonaceous particles. They also compared the features and performance of this instrument to those of a two-colour ratio pyrometer reported earlier [26]. The three-colour ratio pyrometer was also used in their other investigations on the ignition and combustion characteristics of coal particles [2-5]. Riaza et al. [12] investigated the combustion behaviours of four kinds of pulverized biomass samples (sugarcane bagasse, pine sawdust, torrefied pine sawdust and olive residue) in a drop-tube furnace, at 1400K, under both air and oxygen-enriched combustion conditions using the three-colour pyrometry method. The obtained temperature-time profiles of the burning particles were used to deduce the char combustion temperatures.

Comparing to the conventional TGA and optical pyrometry, high-speed cinematography offers a temporal and spatial means for the visualisation and non-intrusive measurement of a high dynamic process such as particle combustion, and consequently the quantitative characterisation of the burning particle, including particle size, shape, ignition, etc. Riaza et al. [12] used a high-speed video camera, at a frame rate of 1 or 2 kHz, fitted with an infinity model K2 long-distance microscope lens to provide high-magnification images of the combustion events. The behaviours of the four types of biomass samples were found to be similar with two phases: the initial volatile flames and the consequential char combustion. Mason et al. [22] used a FujiFilm Finepix HS10 camera for video recording, with a frame rate of 120 Hz, and evaluated the ignition delay, volatile burning time and char burnout time based on the images captured. Carlsson et al. [23] captured the behaviour of biomass particles (European spruce and American hardwood) during pyrolytic reactions by means of high-speed imaging and image processing to track the contour of the biomass particles. Gao et al. [24] proposed a novel instrumentation system, incorporating a colour CCD camera and multi-wavelength laser sources, to achieve the on-line continuous measurement of particle size and shape distributions. In contrast to the single-laser technique, this system was statistically more representative and more reliable. Qian et al. [25] presented the on-line continuous measurement of mean particle velocity, concentration and particle size distribution of pulverized fuel using multi-channel electrostatic sensing and digital imaging techniques. However, most of the previous studies using high-speed cinematography focus on the measurement of particle size, shape, ignition delay, combustion duration time etc. and few, if any, have investigated the luminous intensity of the flame, which may bring new knowledge on the understanding of the biomass particle combustion process. In addition, as recently pointed out by Wang et al. [27], a proper image enhancement technique is essential to the understanding of combustion flames recorded by a high-speed camera.

In present work, high-speed cinematography was used as the main methodology to study the biomass combustion behaviours of both volatile matter and char residue. From the obtained images, the profiles of equivalent flame diameter and average luminous intensity were deduced by means of image processing, which represents a new attempt to derive some of the biomass combustion characteristics as few have done it so far. The combustion durations of volatile matter and char residue were also calculated and analysed.

2. Biomass fuel characteristics and experimental methods

2.1 Physical and chemical properties of the biomass fuel particles

Three different types of biomass fuels were studied: pine pellets, olive residue and eucalyptus pellets. Pine pellets were made from 100% pine sawdust by-product from saw-mills with the timber coming from various sustainable UK forests. The Olive residue with a particle size of less than 1mm was the olive oil by-product. It was a bio-fuel of choice for co-firing in some UK power stations, due to its low cost and the high security of supply. Eucalyptus pellets were obtained from a UK power station which was co-firing the pellets with coal. All the biomass fuels were further ground to less than 212 μm using a Retsch planetary ball mill (PM 100) and sieved to different size ranges. The size cut of 125-150 μm was selected for the experiments on the consideration of problem-free and stable feeding. Proximate analysis of the biomass fuels was carried out according to the European Standards (ISO 18122:2015, ISO 18123:2015, ISO 18134-2:2015); in particular, the volatile matter mass fraction was determined at 1173 K and the ash mass fraction at 823 K. The elemental compositions (C, H, N, S) of the fuel samples were determined using a Thermo Flash EA 1112 Series, whereas the high heating values of the biomass fuels were calculated using the correlation developed by Friedl et al. [28]. Table 1 shows the proximate and ultimate analysis as well as the high heating values of the tested biomass fuels.

(Table 1)

2.2 Experimental setup

2.2.1 Visual Drop-tube furnace (V-DTF)

A visual drop-tube furnace was used for the combustion experiments with the schematic of the experimental setup shown in Fig.1. The furnace was a lab-scale entrained-flow reactor fitted with a 1400 mm long quartz-tube, of which 1000 mm was electrically heated, with an inner diameter of 50mm. There was a slotted side window (30 mmx560 mm), positioned at the mid-section of the furnace, through which the high-speed cinematography could be conducted. A water-cooled feeding probe (internal diameter of 5 mm and length of 760 mm) and a water-cooled collection probe (internal diameter of 15 mm and length of 610 mm), both made of 316 stainless steel, were positioned axially at the top and bottom of the quartz tube. The separation distance between the two probes can be changed but was fixed at 530 mm for the experiments reported in this paper.

For the individual particle combustion tests, a small amount (a few milligrams) of each fuel sample was manually dropped to the furnace through the water-cooled feeding probe without the use of a carrier gas but with the supply of the secondary air at 5 L min^{-1} (Fig.1). The furnace temperature was set at 1073 K and the reactor temperature (measured by a type-R platinum thermocouple enclosed in a high purity alumina protection tube) between the two probes was about 1058 K with a variation of less than 5 K.

(Figure 1)

2.2.2 High-speed camera

A high-speed camera (Phantomv12.1) was used to study the burning of single biomass particles. The camera is capable of recording videos at a frame rate up to 1 MHz. At its full resolution (1280 x 800 widescreen), it can shoot at a frame rate of 6.242 kHz. The camera was fitted with a long distance microscope lens (Questar QM-1), ranging from 56 cm to 152 cm with a resolution of 1.1 μm at 15 cm, to provide high-magnification images of combustion events. The camera was positioned adjacent to the slotted window, with the frame rate of 6.2 kHz throughout the experiments.

Multiple runs of combustion experiments were conducted for each biomass fuel, where some video recordings were discarded due to various reasons such as problematic feeding and blurred recording. From the reserved videos, a minimum of 20 individual burning particles for each fuel, which had the entire combustion process recorded in the video, were selected and analysed in this work as to be described below.

3. Results and Discussion

3.1 Observations on combustion behaviour

A set of snapshot photographic sequences of typical combustion events in air for each biomass sample during burning history are shown in Fig. 2. In order to display the whole combustion process more clearly, image enhancement was performed on all images in Fig. 2. The image enhancement here is the adjustment of grey-scale, which maps the intensity values in grey-scale image to new values. This increases the contrast of the output image in order to help us observe the combustion process more clearly. However, it should be noted the image enhancement was only used in Fig. 2 but not in the calculations of other figures.

(Figure 2)

3.1.1 Eucalyptus

The eucalyptus particles consistently experienced two separate combustion stages. That is, the vast majority of the char residues ignited almost simultaneously (within the interval of less than one millisecond) when the volatile flames extinguished, see Fig.2 (a). Upon a particle being heated up in the V-DTF, the volatile matter ignited, forming a faint (hardly detectable) envelope flame around the particle. Such flames had strikingly spherical shapes, with an increasing luminosity from the centre to edge. As the devolatilisation progressed, the luminosity of the flame enhanced, whereas the size of the particle shrank gradually. Then, the particle accelerated its rotation suddenly and the volatile flame extinguished a couple of milliseconds later. Upon the extinction of the volatile flame, the ignition of char occurred. The solid char combustion event had a much higher intensity than the volatile flame, which was seen from the brightly burning particle. The radiation intensity remained relatively constant with time, but eventually, decreased quickly. During the solid char combustion stage, a number of eucalyptus particles fragmented to several parts and the fragments continued burning until completion.

3.1.2 Pine

The pine particles had similar combustion behaviour with eucalyptus particles, in terms of gas-phase combustion and solid char combustion, as displayed in Fig.2 (b). The volatile envelope flames were distinct and easily discernible from the background. Such flames occurred for a relatively long duration, with the flame size decreasing during the second half of the gas combustion. Suddenly occurred fast rotations of the burning particle were also observed before extinction of the volatile flame. After the ignition of char residue, the burning particle became increasingly luminous and the flame contour became greater along with the extension of the burning surface. Then the flame remained stable in size with high intensity. Afterwards, fragmentations took place for most pine particles.

3.1.3 Olive

The olive particles also exhibited two-phase combustions, however, somewhat differently as shown in Fig.2 (c). Firstly, when the volatile matter was burning, the flame was much fainter than the volatile flames of other two types of biomass fuels and without the notable spherical envelope. Upon the extinction of the volatile flame, the char particle experienced a brief ignition delay period, appearing to be dark for about one millisecond. Then the char ignition occurred at a corner of the particle and spread gradually across the whole surface, with an increased luminosity. A similar conclusion was found by Levendis et al. [29] that the char particles do not ignite over their whole external surface, but exhibit preferential ignition at specific sites. After a period of steady and fast burning, the shrinking core faded away.

The three types of biomass particles shared the behaviour of two evident combustion phases, the volatile combustion in a spherical and low-luminous envelope flame and the high-intensity char residue combustion. The olive residue had a fainter volatile flame than pine and eucalyptus due to its high ash mass fraction. During the char combustion phase, fragmentation took place for all three types of biomass particles but more often for pine particles. Some of the combustion characteristics of biomass particles seen in this study were also observed by other researchers [2, 12], including the sequential particle devolatilisation with ignition and burning of the volatiles around the particle, followed by the ignition, combustion and extinction of the char residue.

3.2 Flame contour

For each combustion event, a group of frames from the high-speed video were imported to Matlab. Otsu's method [30] was used to convert a grey-level image to a binary image by calculating the optimum threshold.

Fig.3 shows the typical profiles of flame contours during their entire burning history, deduced using image processing. Since both the volatile flame and burning char were irregularly shaped, the contour area can generally be represented in terms of an equivalent diameter. This was achieved by transforming the contour area to its equivalent circle which has the same number of pixels of the contour area. The equivalent diameter was then defined as the diameter of the equivalent circle.

(Figure 3)

The profiles of the flame equivalent diameter shown in Fig.3 indicate that the three kinds of biomass particles were all burning in two distinct phases, one with a relatively large volatile combustion flame and the other with a small luminous burning char body, agreeing with the visual observations described in Section 3.1. Fig.3 also illustrates that, for pine and eucalyptus particles, the diameter of the volatile matter combustion flame (60 pixels) was about twice as large as that of the char body (30 pixels). Olive extended the disparity in the equivalent diameter to about five times. A similar trend was found by Khatami et al. [31] who had tested three types of biomass particles (bagasse, pine sawdust and olive residue) within the range of 75-150 μm and found the peak size of the envelope flame was around 190-300 μm. For all three kinds of biomass particles, the flame size decreased slowly during most of the char combustion stage and then experienced a dramatic decline shortly before the final burn-off, which indicates shrinking core combustion behaviour. Previous work by Levendis et al. [2] and Khatami et al. [4] reported that sugarcane bagasse particles also exhibited a shrinking core behaviour during the char combustion stage.

3.3 Average luminous intensity

The profiles of the average luminous intensity during the entire combustion process of each biomass fuel were also deduced by analysing the recorded images frame by frame as shown in Fig.4. The luminous intensity values were expressed by the mean grey values of all pixels within the flame contours.

(Figure 4)

For all fuels, the char combustion phases were easily identified by the conspicuously large values of the average luminous intensity. In all cases, the char combustion phases were much more luminous. For pine and olive particles, the average luminous intensity could reach the peak value of almost 100 in grey value but for the eucalyptus particles, it could only reach about 70. The aforementioned phenomenon that the olive volatile matter burning with a quite fainter (with a value of no more than 10) flame than the other two biomass fuels (with a value of more than 20) could also be noticed on the luminous intensity profiles (Fig.4). These indicate that the eucalyptus particles burned at a lower temperature than pine and olive particles under the same V-DTF setup conditions (at 1073 K furnace temperature and in air) despite the fact that eucalyptus has the highest volatile matter mass fraction. The rapid release of the larger cloud of volatiles with the eucalyptus particles may have retarded the diffusion of O_2 and hence lead to lower combustion temperatures at both the volatile and char combustion stages.

It is worth noting that there are two peak values in both the equivalent diameter (Fig.3) and the average luminous intensity (Fig.4) during the devolatilisation/volatile combustion stages of the pine and eucalyptus particles, which were not observed by means of optical pyrometry according to a previous study [12]. Riaza et al. [12] investigated the combustion of single particles of four kinds of biomasses (sugarcane bagasse, pine sawdust, torrefied pine sawdust and olive residue) by use of a drop-tube furnace and three-colour pyrometry. They found that the first three types of biomass particles only had one pyrometric peak during the volatiles combustion stage. In addition, the pyrometric peak of the olive's volatiles combustion was found to be much weaker than that of other biomass samples. Some analogous but not quite equivalent observations of the two peaks shown in Figs. 3-4 could be found with thermogravimetric analysis as shown in Fig.5. The same biomass fuels were combusted in air in a TGA at a ramp rate of 3 K min^{-1} to elucidate the temperatures at which changes in fuel mass occurred. All of the biomass fuels were found to have multiple peaks in the burnout analysis. Furthermore, during the devolatilisation stage, the olive residue and eucalyptus gave two clear peaks relating to the expected devolatilisation of hemicellulose and cellulose [32]. For the pine particles, the other volatile peak, not detectable, was assumed to be subsumed by the main peak (Fig. 5), which may be confirmed by the much smaller value of the first peak than the second one in Fig.4 (b). Therefore, the observed two peaks of the eucalyptus and pine particles during the volatile combustion stage (Figs. 3-4) in V-DTF also likely indicated the devolatilisation of hemicellulose and cellulose. The expected two peaks of the olive particles could not be observed due to the extremely faint volatile flame as mentioned in Section 3.1.3.

(Figure 5)

3.4 Volatile combustion time and char burnout time

The volatile combustion time and the char burnout time were estimated from both of the cinematographic observations (in Section 3.1) and the profiles of luminous intensity (in Section 3.3). The mean values and standard deviations for all cases were calculated, from a minimum of 20 samples for each fuel. It was found that the combustion time of each particle varied considerably because of different sizes and shapes, although they were ground and sieved to 125-150 μm. To ensure that the particle sizes are basically identical, a small number of the particles with the volatile combustion time and the char burnout time far beyond the standard deviations were removed from the data set. Then the final average values and standard deviations were recalculated and shown in Table 2.

(Table 2)

Fig.6 gives the total number of burning particles finally used for the analysis shown in Table 2. It can be seen from Fig. 6 that there was a little correlation between the volatile combustion time and the char burnout time for any of the three biomass fuels.

(Figure 6)

Intuitively one would expect that the volatile combustion time would increase with the volatile matter mass fraction of the fuel and the char burnout time would increase with the fixed carbon mass fraction of the fuel. Contrary to this expectation, the volatile combustion time shown in Fig.7 decreased slightly with the volatile matter mass fraction. There are a number of possible reasons for this observation. Firstly, the determination of the precise initial instance of the volatile ignition was difficult because of the low luminosity of the volatile envelope flame thus low contrast with the background. Secondly, the process of the visible volatile combustion did not cover the entire period of the devolatilisation that should start much earlier than the volatile flame becoming visible. Thirdly, the olive residue has a much higher ash mass fraction than the other two fuels, which may influence the combustion behaviour of the volatile matter. Riaza et al. [12] also pointed out that the olive residue had a lower temperature and less-influenced char burnout time compared to other biomass fuels because of its high ash mass fraction.

(Figure 7)

Fig. 8 shows the relationship between the char burnout time and the fixed carbon mass fraction of the fuels. It shows clearly that the char burnout time increases with the fixed carbon mass fraction of the fuel as expected and agrees with the findings of Riaza et al. [5]. The olive residue has the highest fixed carbon mass fraction and thus exhibited the longest char combustion time, whereas eucalyptus had a fixed carbon mass fraction of about half of that of the olive residue and pine, and exhibited a much shorter char burnout time.

(Figure 8)

Although the three biomass fuels were ground and sieved to the size cut of 125-150 μm, the particles can differ not only in sizes but also in shapes which could be spherical, cylindrical or even needle-shaped. The sizes and shapes of the particles would certainly have influenced the combustion characteristics of the fuels, particularly the durations of volatile combustion and char burnout. To minimize the influence of the particle size and shapes on the observed combustion of volatiles and char, the ratio between the char burnout time and the volatile combustion time, was used for further analysis in this study. Fig. 9 shows clearly that the ratio between the char burnout time and the volatile combustion time was well correlated with the fixed carbon to volatile matter mass ratio. This confirms that the char combustion is a much slower process than the volatile combustion process. Fig. 9 also agrees with Riaza et al.[5] who found the dependency of char burnout times versus the fixed carbon mass fraction was quadratic for air and lower oxygen mole fractions in CO_2 (21%O_2).

(Figure 9)

4. Conclusions

This research has demonstrated that the combination of the visual drop tube furnace and the high-speed cinematography with image processing can be an excellent tool to study the combustion characteristics of individual pulverised biomass particles. All three kinds of biomass samples (pine, olive and eucalyptus) have shown two burning phases consisting of the enveloped faint volatile combustion phase and the bright, relatively stable char combustion phase. The two peak values in the profiles of the flame size and the average luminous intensity during the volatile combustion process of pine and eucalyptus particles appear to correspond to the devolatilisation of hemicellulose and cellulose, and this represents new insight to the understanding of the volatile combustion process of biomass. Furthermore, the ratio between the estimated char burnout time and volatile combustion time increases quadratically with the fixed carbon to volatile matter mass ratio, confirming that the char combustion is a much slower process than the volatile combustion process.

Acknowledgments

This work was supported by the UK Engineering and Physical Sciences Research Council [grant number: EP/G037345/1], the UK Carbon Capture and Storage Research Centre [EP/K000446/1, EP/K000446/2, Call 1 Project: C1-27], Doosan Babcock Ltd., Scottish and Southern plc. (SSE), the National Natural Science Foundation of China [51404223, 51476154] and the Natural Science Foundation of Zhejiang Province, China [LQ14E060003, LY13E060006]. China Scholarship Council is also acknowledged for sponsoring Liang Shan and Ming Kong to complete part of the work at the University of Nottingham.

References

[1] A. Malmgren, G. Riley, in: Dermot J. Roddy (Eds.), 5.04 - Biomass Power Generation, Elsevier, 2012, p.27, doi:10.1016/B978-0-08-087872-0.00505-9

[2] Y.A. Levendis, K. Joshi, R. Khatami, A.F. Sarofim, Combustion behavior in air of single particles from three different coal ranks and from sugarcane bagasse, Combustion and Flame. 158 (2011) 452-465.

[3] R. Khatami, C. Stivers, Y.A. Levendis, Ignition characteristics of single coal particles from three different ranks in O2/N2 and O2/CO2 atmospheres, Combustion and Flame. 159 (2012) 3554-3568.

[4] R. Khatami, C. Stivers, K. Joshi, Y.A. Levendis, A.F. Sarofim, Combustion behavior of single particles from three different coal ranks and from sugar cane bagasse in O2/N2 and O2/CO2 atmospheres, Combustion and Flame. 159 (2012) 1253-1271.

[5] J. Riaza, R. Khatami, Y.A. Levendis, L. álvarez, M.V. Gil, C. Pevida, F. Rubiera, J.J. Pis, Single particle ignition and combustion of anthracite, semi-anthracite, and bituminous coals in air and simulated oxy-fuel conditions, Combustion and Flame. 161 (2014) 1096-1108.

[6] R. Khatami, Y.A. Levendis, M.A. Delichatsios, Soot loading, temperature and size of single coal particle envelope flames in conventional- and oxy-combustion conditions (O2/N2 and O2/CO2), Combustion and Flame. 162 (2015) 2508-2517.

[7] L.D.Timothy, A.F. Sarofim, J.M. Beer, Characteristics of single particle coal combustion, Symposium (International) on Combustion. 19 (1) (1982) 1123-1130.

[8] P.A. Bejarano, Y.A. Levendis, Single-coal-particle combustion in O2/N2 and O2/CO2 environments, Combustion and Flame. 153 (2008) 270-287.

[9] A. Atal, Y.A. Levendis, Comparison of the combustion behaviour of pulverized waste tyres and coal, Fuel. 74 (11) (1995) 1570-1581.

[10] Y.A. Levendis, K.R. Estrada, H.C. Hottel, Development of multicolor pyrometers to monitor the transient response of burning carbonaceous particles, Review of Scientific Instruments. 63 (7) (1992) 3608-3622.

[11] M. Loewenberg, Y.A. Levendis, Combustion behavior and kinetics of synthetic and coal-derived chars: comparison of theory and experiment, Combustion and Flame. 84 (1991) 47-65.

[12] J. Riaza, R. Khatami, Y.A. Levendis, L. A´lvarez, M.V. Gil, C.Pevida, F. Rubiera, J.J. Pis, Combustion of single biomass particles in air and in oxy-fuel conditions, Biomass and Bioenergy. 64 (2014) 162-174.

[13] A. Toptas, Y. Yildirim, G. Duman, J. Yanik, Combustion behavior of different kinds of torrefied biomass and their blends with lignite, Bioresource Technology. 177 (2015) 328-336.

[14] X. Liu, M.Q. Chen, Y.H. Wei, Combustion behavior of corncob/bituminous coal and hardwood/bituminous coal, Renewable Energy. 81 (2015) 355-365.

[15] Y.H. Wei, M.Q. Chen, S.B. Niu, F. Xue, Experimental investigation on the oxy-fuel co-combustion behavior of anthracite coal and spent coffee grounds, Journal of Thermal Analaysis and Calorimetry. 124 (2016) 1651–1660.

[16] Y. Haseli, J.A. van Oijen, L.P.H. de Goey, A detailed one-dimensional model of combustion of a woody biomass particle, Bioresource Technology. 102 (2011) 9772-9782.

[17] Y.B. Yang, V.N. Sharifi, J. Swithenbank, L. Ma, L.I. Darvell, J.M. Jones, M. Pourkashanian, A. Williams, Combustion of a single particle of biomass, Energy and Fuels. 22 (1) (2008) 306-316.

[18] H. Lu, W. Robert, G. Peirce, B. Ripa, L.L. Baxter, Comprehensive study of biomass particle combustion, Energy and Fuels. 22 (4) (2008) 2826-2839.

[19] H. Thunman, B. Leckner, F. Niklasson, F. Johnsson, Combustion of wood particles-a particle model for Eulerian calculations, Combustion and Flame. 129 (2002) 30-46.

[20] O. Karlström, A. Brink, M. Hupa, Time dependent production of NO from combustion of large biomass char particles, Fuel. 103 (2013) 524-32.

[21] J. Li, M.C. Paul, P.L. Younger, I. Watson, M. Hossain, S. Welch, Characterization of biomass combustion at high temperatures based on an upgraded single particle model, Applied Energy. 156 (2015) 749-755.

[22] P.E. Mason, L.I. Darvell, J.M. Jones, M. Pourkashanian, A. Williams, Single particle flame-combustion studies on solid biomass fuels, Fuel. 151 (2015) 21-30.

[23] P. Carlsson, H. Lycksam, P. Gren, R. Gebart, H. Wiinikka, K. Iisa, High-speed imaging of biomass particles heated with a laser, Journal of Analytical and Applied Pyrolysis. 103 (2013) 278–286.

[24] L.J. Gao, Y. Yan, G. Lu, R.M. Carter, On-line measurement of particle size and shape distributions of pneumatically conveyed particles through multi-wavelength based digital imaging, Flow Measurement and Instrumentation. 27 (2012) 20-28.

[25] X.C. Qian, Y. Yan, L.J. Wang, J.Q. Shao, An integrated multi-channel electrostatic sensing and digital imaging system for the on-line measurement of biomass-coal particles in fuel injection pipelines, Fuel. 151 (2015) 2-10.

[26] Y.A. Levendis, A fundamental study of char oxidation kinetics using model materials, Doctor of Engineering Thesis, California Institute of Technology, 1988.

[27] Y.Wang, L.Zheng, R.Woolley, Y.Zhang, Investigation of ignition process from visible to infrared by a high speed colour camera, Fuel. 185(2016) 500-507.

[28] A. Friedl, E. Padouvas, H. Rotter, K. Varmuza, Prediction of heating values of biomass fuel from elemental composition, Analytica Chimica Acta. 544 (2005) 191–198.

[29] Yiannis A. Levendis, Ranajit Sahut, Richard C. Flagan and George R. Gavalas, Post-ignition transientsof single char particles, Fuel. 68(1989) 849-855.

[30] N. OTSU, A Threshold Selection Method from Gray-Level Histograms, IEEE Transactions on Systems, Man, and Cybernetics. 9 (1) (1979) 62-66.

[31] R. Khatami, Y.A. Levendis, An overview of coal rank influence on ignition and combustion phenomena at the particle level, Combustion and Flame. 164 (2016) 22–34.

[32] C.C. Zhou, G.J. Liu, X.D. Wang, C.C. Qi, Co-combustion of bituminous coal and biomass fuel blends: Thermochemical characterization, potential utilization and environmental advantage, Bioresource Technology. 218 (2016) 418-427.

List of captions

Table 1 Proximate and ultimate analysis of the biomass fuels

Table 2 Average volatile combustion time and char burnout time of three biomass fuels

Figure 1 Schematic of the experimental setup

Figure 2 Images of combustion sequence of single biomass particles (zero millisecond merely represents the beginning of the visible ignition of the volatile matter) (a) Eucalyptus, (b) Pine, (c) Olive

Figure 3 Equivalent diameter of flame contour versus time (a) Eucalyptus, (b) Pine, (c) Olive

Figure 4 Average luminous intensity of particle flames versus time (a) Eucalyptus, (b) Pine, (c) Olive

Figure 5 Comparison of ignition of biomass fuels using TGA (air, 3°C min^{-1})

Figure 6 Average volatile combustion time versus char burnout time

Figure 7 Average volatile combustion time versus volatile matter mass fraction

Figure 8 Average char burnout time versus fixed carbon mass fraction

Figure 9 The ratio between char burnout time and volatile combustion time versus the volatile matter and fixed carbon mass ratio

Table 1 Proximate and ultimate analysis of the biomass fuels*

Biomass		Eucalyptus#	Olive residue#	Pine#
Proximate analysis (mass fraction%, db or ar) FC determined by difference	M_{ar}	5.9	6.2	4.4
	VM_{db}	88.3	71.5	83.8
	FC_{db}	8.7	16.1	15.6
	Ash_{db}	3.0	12.4	0.6
Ultimate analysis (mass fraction%, db) O determined by difference	C	48.7	45.9	48.0
	H	5.7	5.7	5.9
	O	42.4	33.9	45.3
	N	0.2	2.1	0.2
	S	nd	nd	nd
HHV(MJ kg^{-1} db)		20.7	18.4	20.0

* 'FC'=fixed carbon, 'M'='Moisture, 'VM'=Volatile Matter, 'ar'=as received, 'db'=dry basis, 'nd'=not detected. Proximate Analysis – according to the European Standards for solid biofuels (ISO 18122:2015, ISO 18123:2015, ISO 18134-2:2015).
# This work was performed on substrates of unknown provenance, for which the chain of custody is not known. The species are known but the cultivars cannot be specified and while the authors believe that this work exemplifies the difference between the species - there is a reasonable concern that there may be substrate factors and handling chain factors that could influence the results obtained.

Table 2 Average volatile combustion time and char burnout time of three biomass fuels

	Volatile combustion time		Char burnout time	
	Mean value (ms)	Standard deviation (ms)	Mean value (ms)	Standard deviation (ms)
Eucalyptus	16.8	3.3	17.0	3.4
Pine	19.7	6.5	27.0	8.0
Olive	20.5	4.6	36.3	8.6

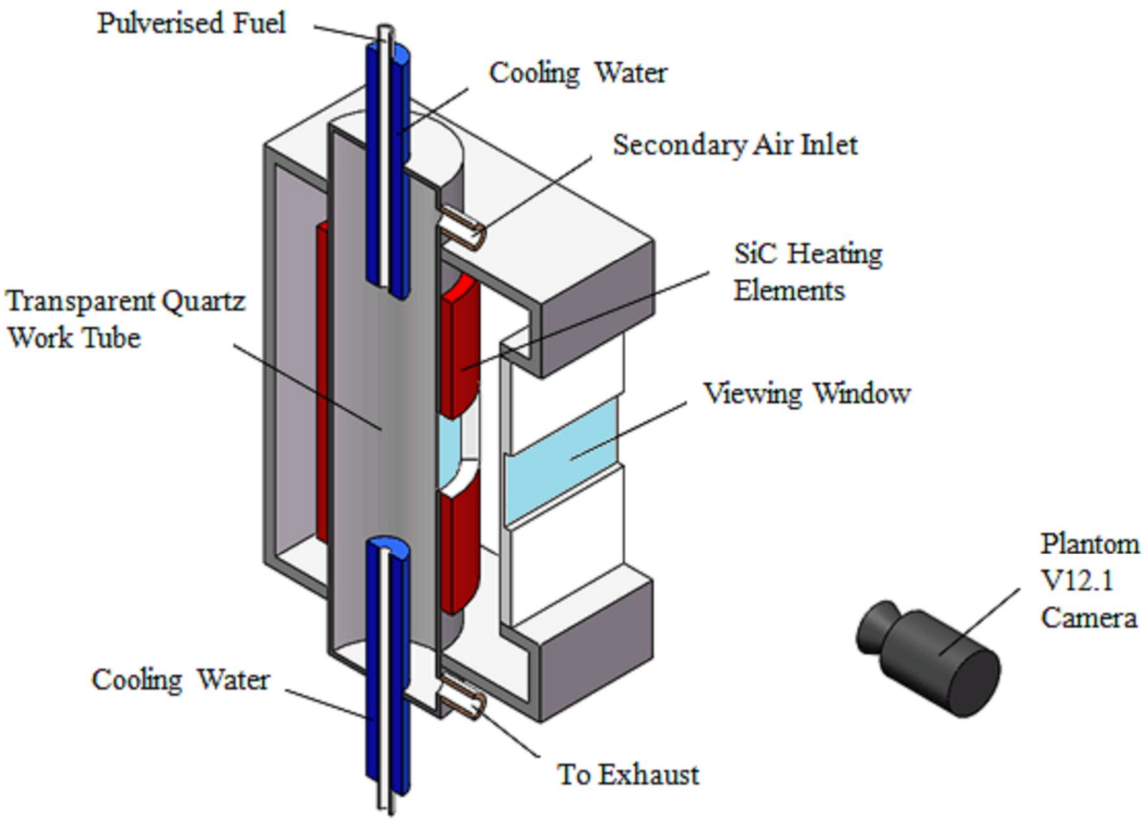

Figure 1

(a)

(b)

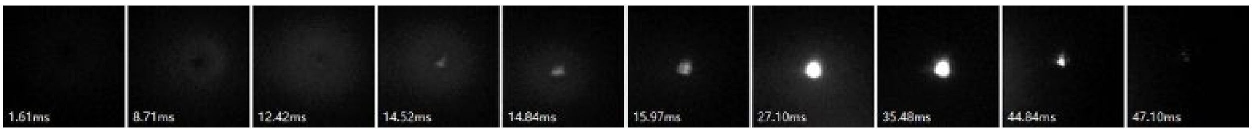

(c)

Figure 2

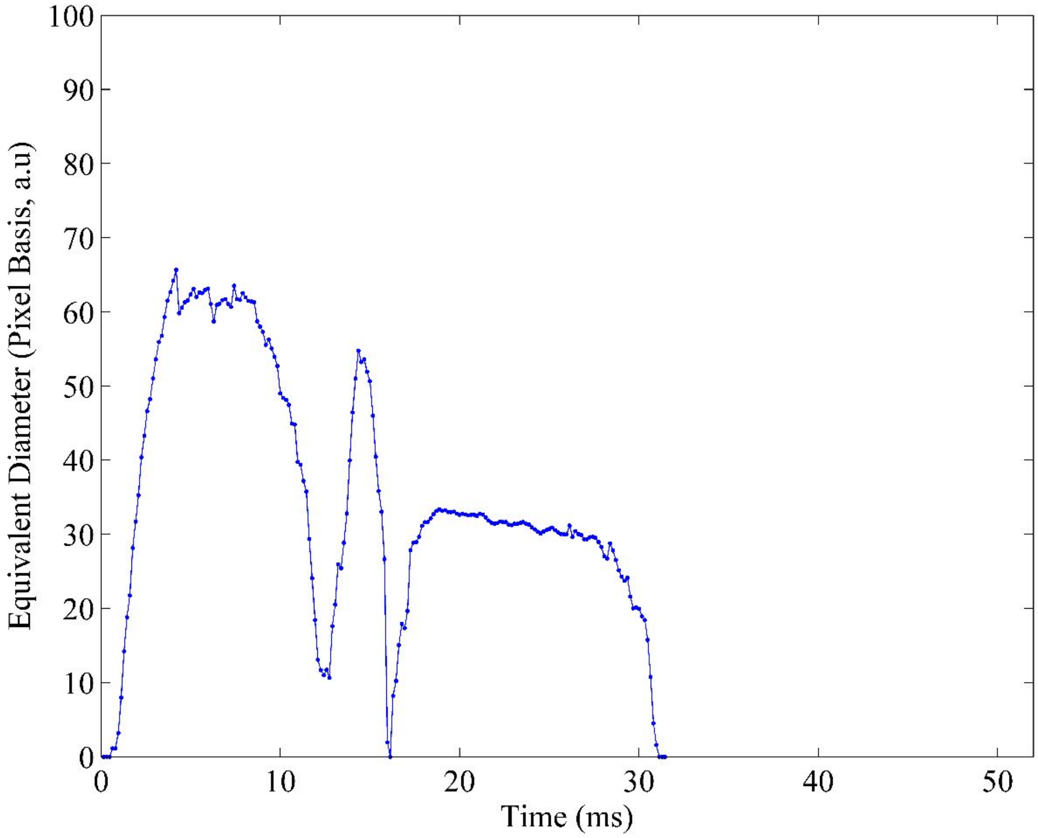

100
90
80
70
60
50
40
30
20
10
0
Equivalent Diameter (Pixel Basis, a.u)
0
10
20
30
40
50
Time (ms)

(a)

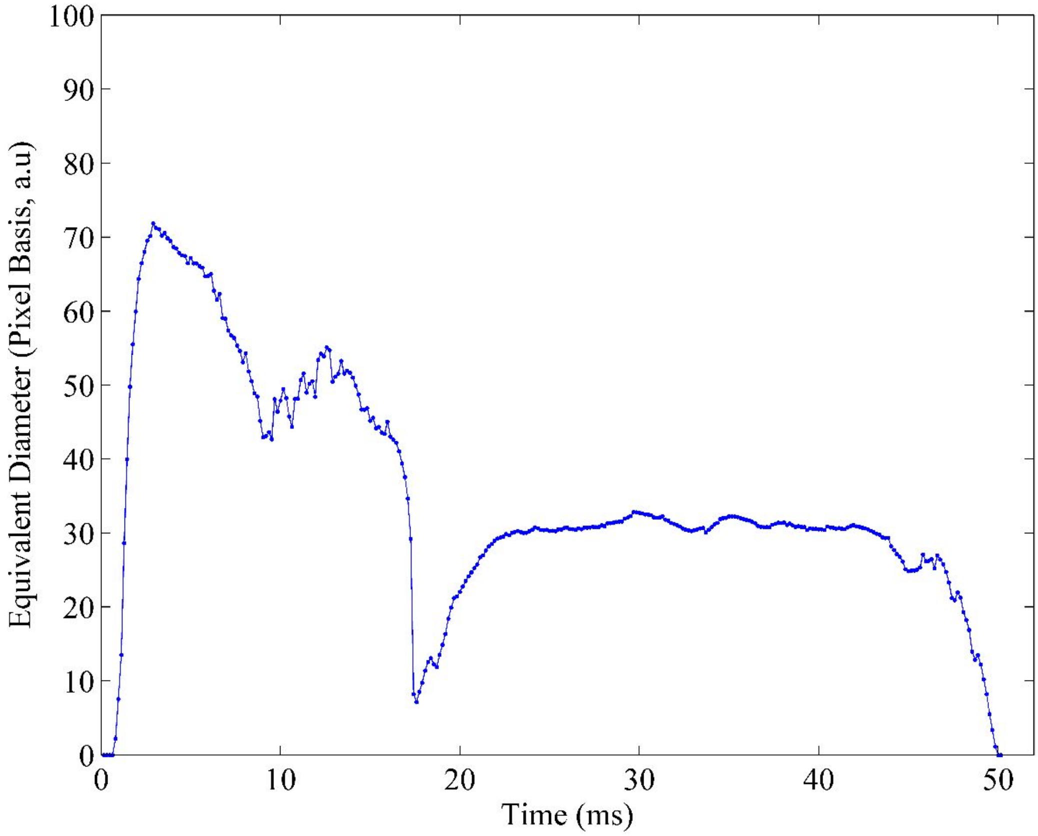
Equivalent Diameter (Pixel Basis, a.u)
Time (ms)
100
90
80
70
60
50
40
30
20
10
0
0
10
20
30
40
50

(b)

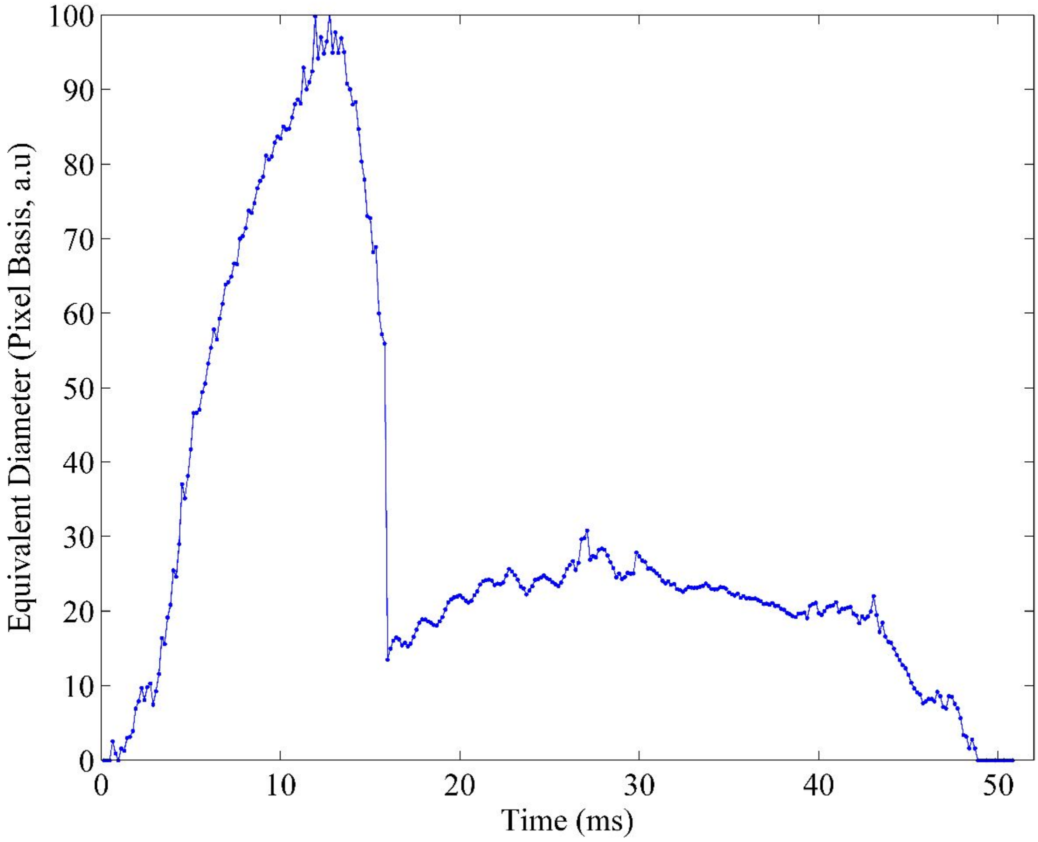

Equivalent Diameter (Pixel Basis, a.u)
Time (ms)
100
90
80
70
60
50
40
30
20
10
0
0
10
20
30
40
50

(c)

Figure 3

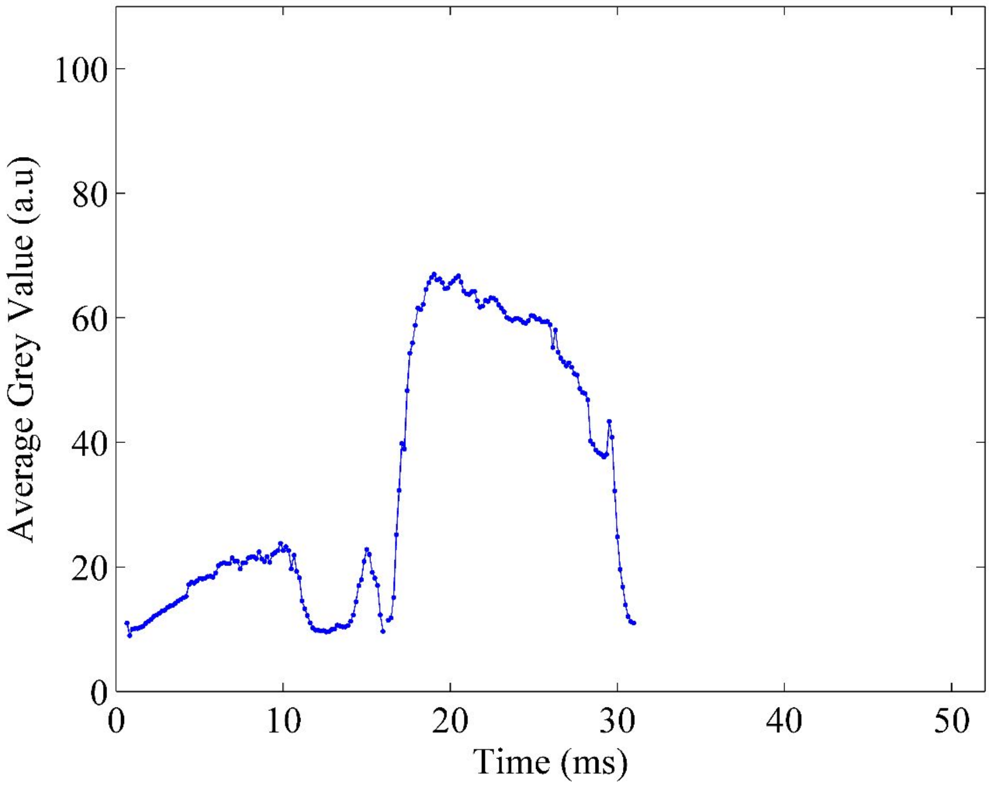

100
80
60
40
20
0
0
10
20
30
40
50
Average Grey Value (a.u)
Time (ms)

(a)

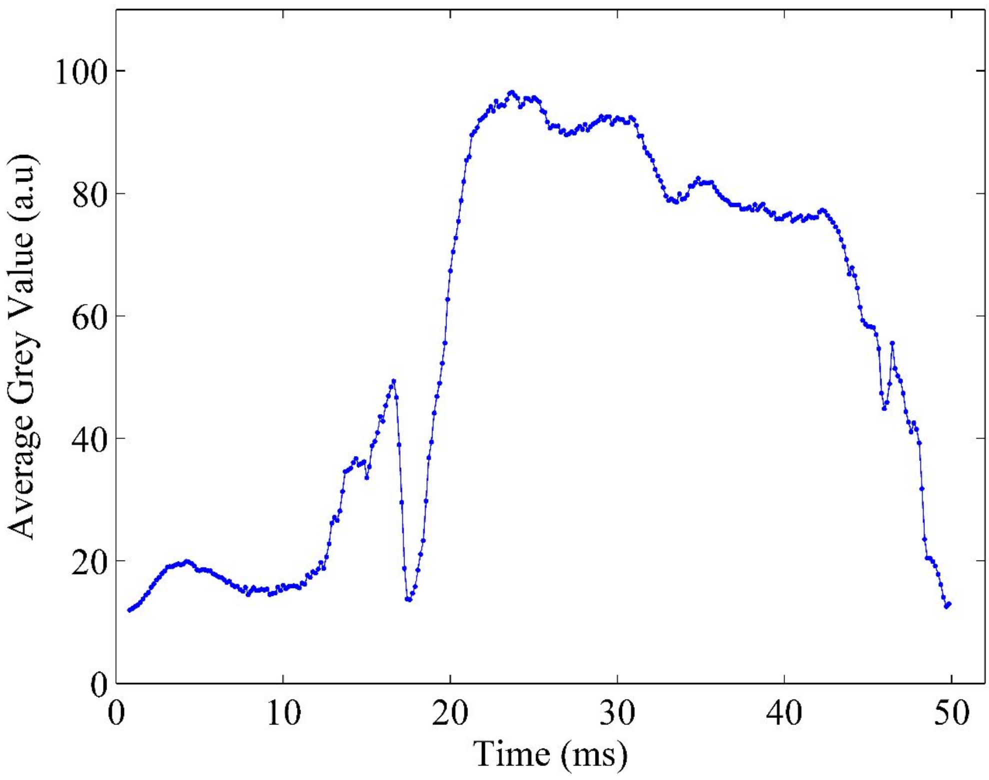

100
80
60
40
20
0
0
10
20
30
40
50
Average Grey Value (a.u)
Time (ms)

(b)

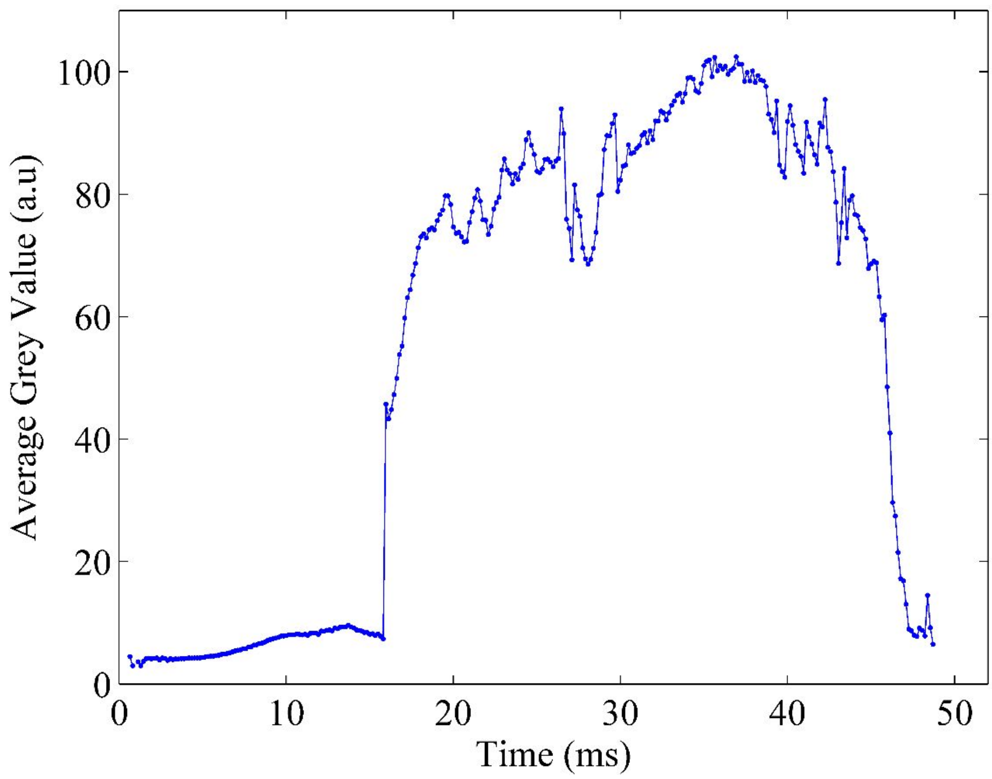

(c)

Figure 4

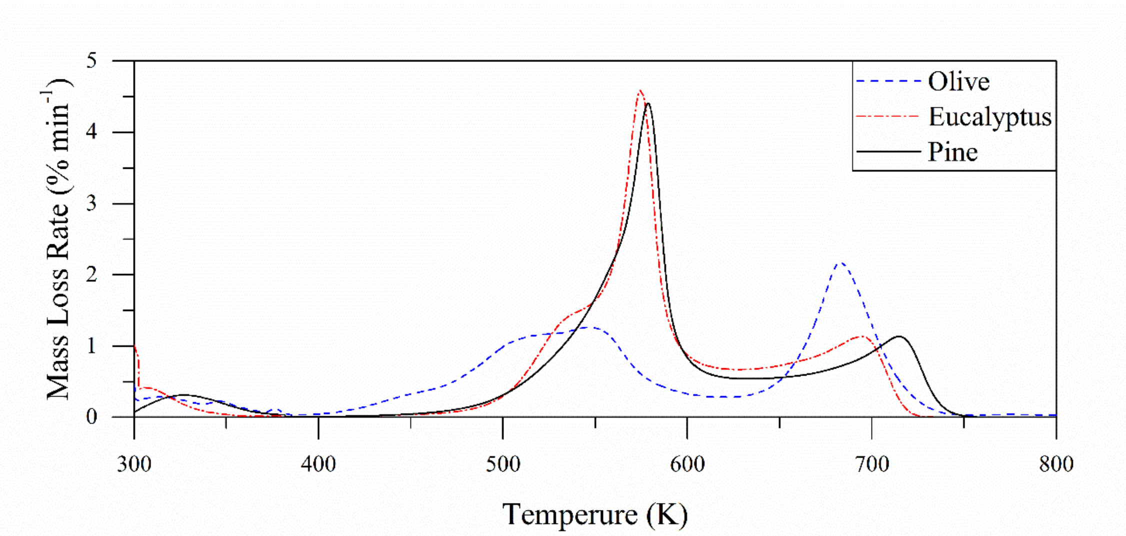

Figure 5

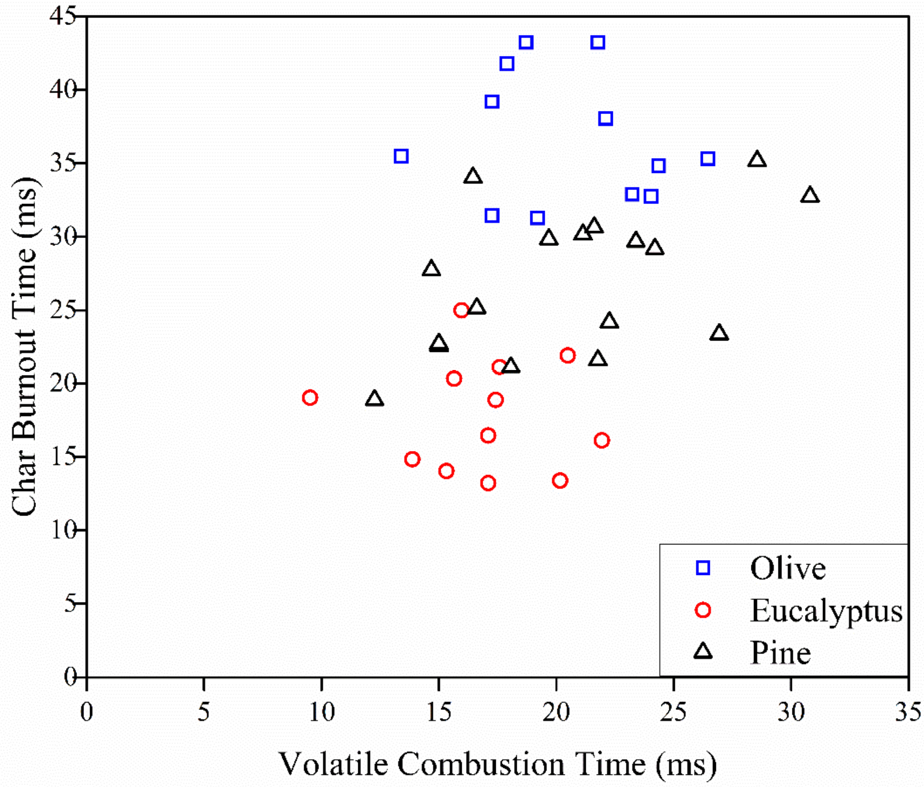

Char Burnout Time (ms)
Volatile Combustion Time (ms)
Olive
Eucalyptus
Pine
0
5
10
15
20
25
30
35
40
45

Figure 6

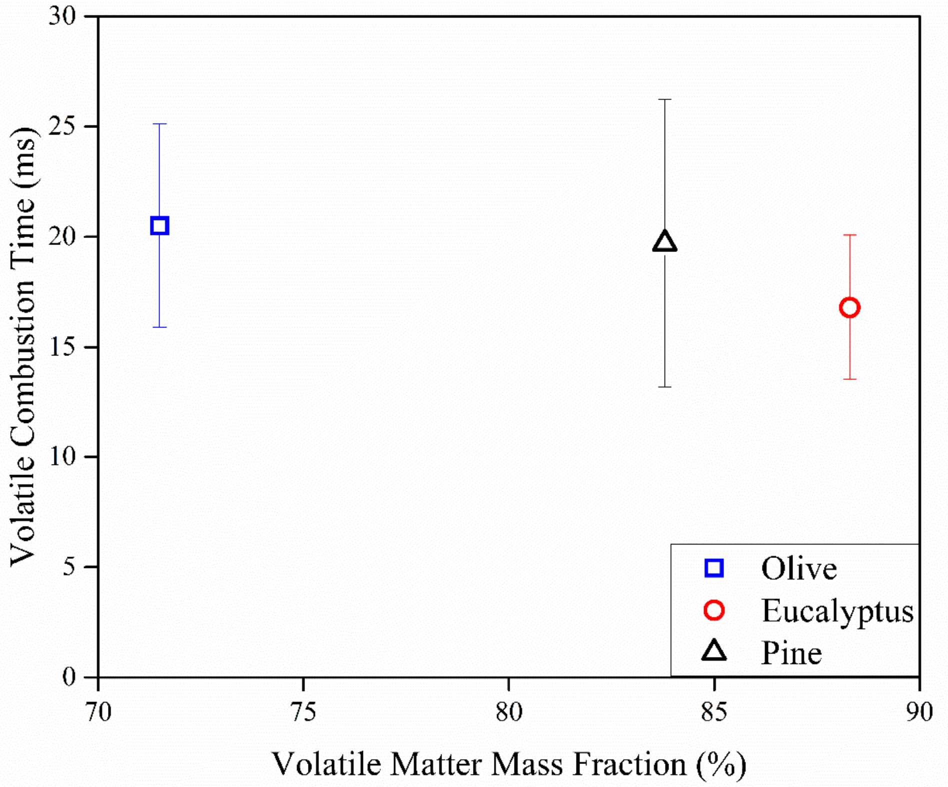

Volatile Combustion Time (ms)
30
25
20
15
10
5
0
70
75
80
85
90
Volatile Matter Mass Fraction (%)
Olive
Eucalyptus
Pine

Figure 7

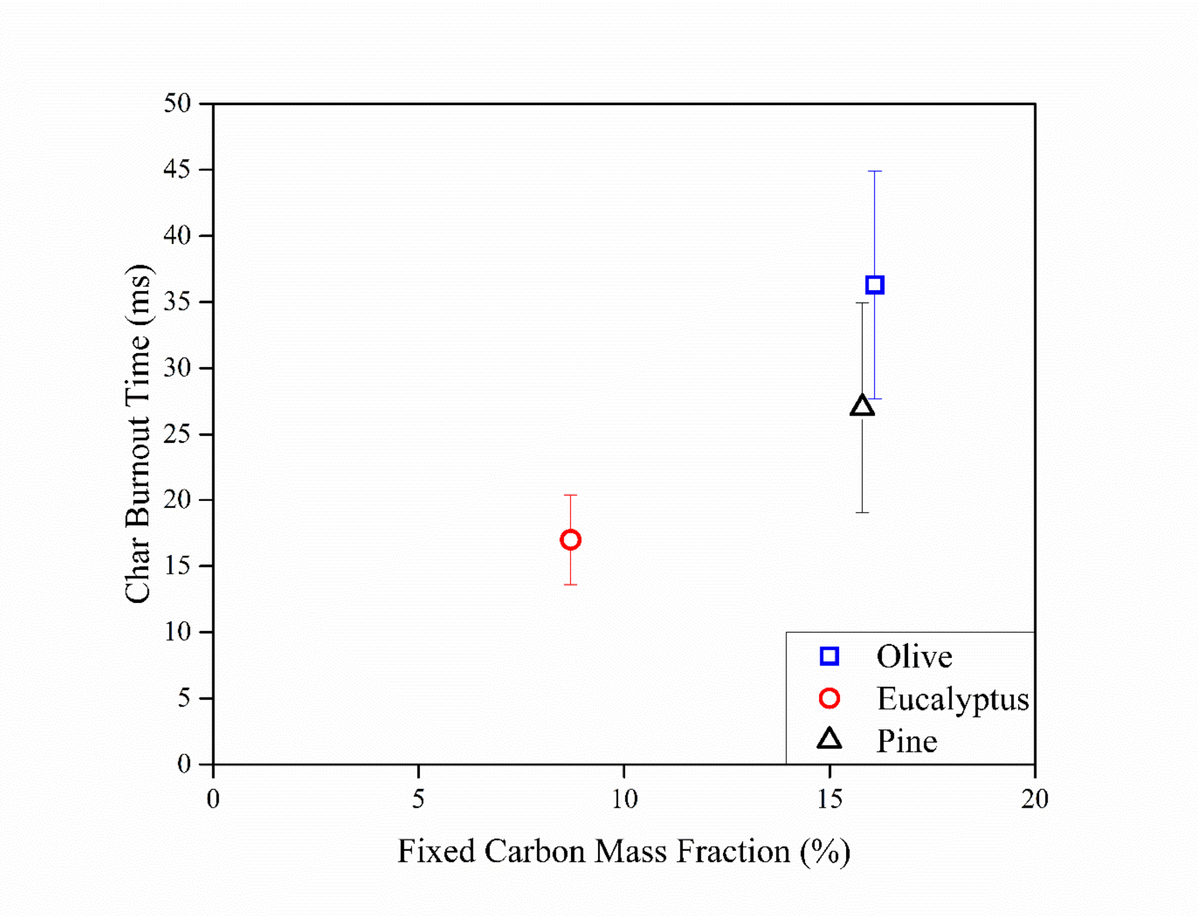

Char Burnout Time (ms)
50
45
40
35
30
25
20
15
10
5
0
0
5
10
15
20
Fixed Carbon Mass Fraction (%)
Olive
Eucalyptus
Pine

Figure 8

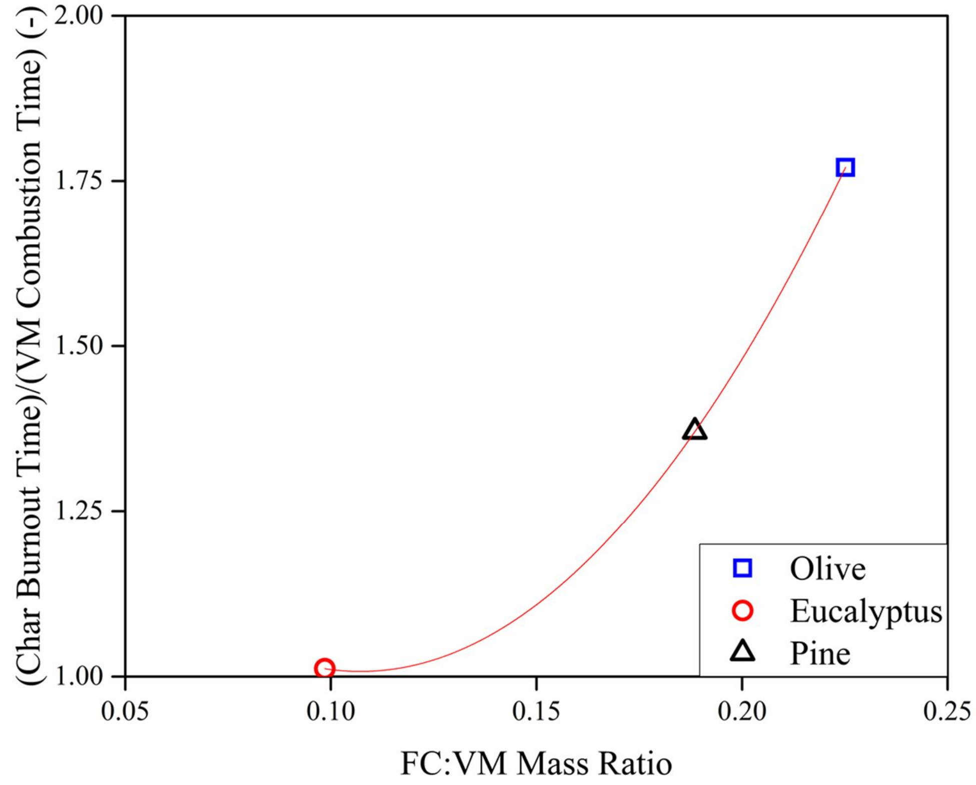
(Char Burnout Time)/(VM Combustion Time) (-)
2.00
1.75
1.50
1.25
1.00
0.05
0.10
0.15
0.20
0.25
FC:VM Mass Ratio
Olive
Eucalyptus
Pine

Figure 9